

Oxygen adsorption structures on Ag(111)

Joachim Schnadt,^{1,2,*} Jan Knudsen,² Xiao Liang Hu,³ Angelos Michaelides,^{3,4} Ronnie T. Vang,² Karsten Reuter,⁴ Zhesen Li,⁵ Erik Lægsgaard,² Matthias Scheffler,⁴ and Flemming Besenbacher^{2,†}

¹*Division of Synchrotron Radiation Research, Department of Physics,
Lund University, Box 118, 221 00 Lund, Sweden*

²*Interdisciplinary Nanoscience Center (iNANO) and Department of Physics and Astronomy,
University of Aarhus, Building 1521, Ny Munkegade, 8000 Aarhus C, Denmark*

³*London Centre for Nanotechnology and Department of Chemistry,
University College London, London WC1E 6BT, UK*

⁴*Fritz-Haber-Institut der Max-Planck-Gesellschaft, Faradayweg 4-6, 14195 Berlin, Germany*

⁵*Institute for Storage Ring Facilities at the University of Aarhus (ISA),
Building 1525, Ny Munkegade, 8000 Aarhus C, Denmark*

(Dated: July 19, 2022)

The oxidized Ag(111) surface has been studied by a combination of experimental and theoretical methods, scanning tunneling microscopy (STM), x-ray photoelectron spectroscopy (XPS), and density functional theory (DFT). A large variety of different surface structures is found, depending on the detailed preparation conditions. The observed structures fall into four classes: (a) individually chemisorbed atomic oxygen atoms, (b) three different oxygen overlayer structures, including the well-known $p(4 \times 4)$ phase, formed from the same Ag_6 and Ag_{10} building blocks, (c) a new $c(4 \times 8)$ structure not previously observed, and (d) at higher oxygen coverages structures characterized by stripes along the high-symmetry directions of the Ag(111) substrate. Our analysis provides a detailed explanation of the atomic-scale geometry of the $\text{Ag}_6/\text{Ag}_{10}$ building block structures, and the $c(4 \times 8)$ and stripe structures are discussed in detail. The observation of many different and co-existing structures implies that the O/Ag(111) system is characterized by a significantly larger degree of complexity than previously anticipated, and this will impact our understanding of oxidation catalysis processes on Ag catalysts.

PACS numbers: 68.43.Bc, 68.37.Ef

I. INTRODUCTION

The oxidation of the Ag(111) surface is a fascinating example of how a seemingly simple system can escape a detailed understanding for decades, in spite of repeated and thorough efforts. The history of surface science investigations of the oxidation of Ag(111), briefly reviewed recently,¹ started back in the sixties and early seventies with a couple of single crystal studies^{2,3,4} and took a serious upswing with the investigations by Rovida *et al.* in the seventies,^{5,6} who, in particular, reported on the now renowned $p(4 \times 4)$ phase. In the following much of the effort was directed towards this phase,^{1,7,8,9,10,11,12,13,14,15,16,17,18,19,20,21} but also numerous other studies of more general character appeared,^{7,8,10,13,16,21,22,23,24,25,26,27,28,29,30,31,32,33,34,35,36,37,38,39,40,41,42,43} as well as works concerned with the reactivity of O/Ag(111) towards, in particular, the oxidation of ethene and methanol.^{44,45,46,47,48,49,50,51,52,53,54,55,56,57,58,59,60,61,62} Only recently the atomic-scale geometric model for the $p(4 \times 4)$ phase was completely revised on the basis of a combination of new scanning tunnelling microscopy (STM), surface x-ray diffraction (SXRD), and x-ray photoemission spectroscopy (XPS) experiments and density functional theory calculations.^{19,20} Subsequent, detailed low-energy electron diffraction and CO reaction studies supported this new atomic model.^{43,63} At the same time

an increasing number of studies have indicated that the phase diagram of the oxidized Ag(111) surface is more complex than previously anticipated. While earlier studies only stipulated the existence of the $p(4 \times 4)$ and an atomic adsorbate layer (including a $p(\sqrt{3} \times \sqrt{3})\text{R}30^\circ$ structure), recent studies have reported phases containing both less,^{12,19,21} equally much,¹⁹ and more⁴² oxygen than the $p(4 \times 4)$ phase. Many of the reactivity studies have assumed that the catalytical properties of Ag are associated with the $p(4 \times 4)$ structure due to the anticipation that this phase should be predominant under oxygen pressures similar to those under reaction conditions.^{14,15} These investigations have in general not taken into account the existence of further phases and, hence, a much more complex phase diagram for the Ag-O system will fundamentally change our picture of what happens in the catalytic process. At present, growing evidence exists that the static phases found in surface science studies may neither be responsible for the surface's catalytic activity itself nor be preserved during catalytic operation.^{21,64,65,66,67} The surface is rather to be considered as a dynamic medium, the structure of which changes in response to the changing chemical environment. The formation and breakup of these static Ag-O phases are still of significant interest due to the phases' role in the overall dynamics of the catalytic process. Thus surface science studies with their unprecedented ability of clarifying the atomic-scale structure still retain their value and validity.

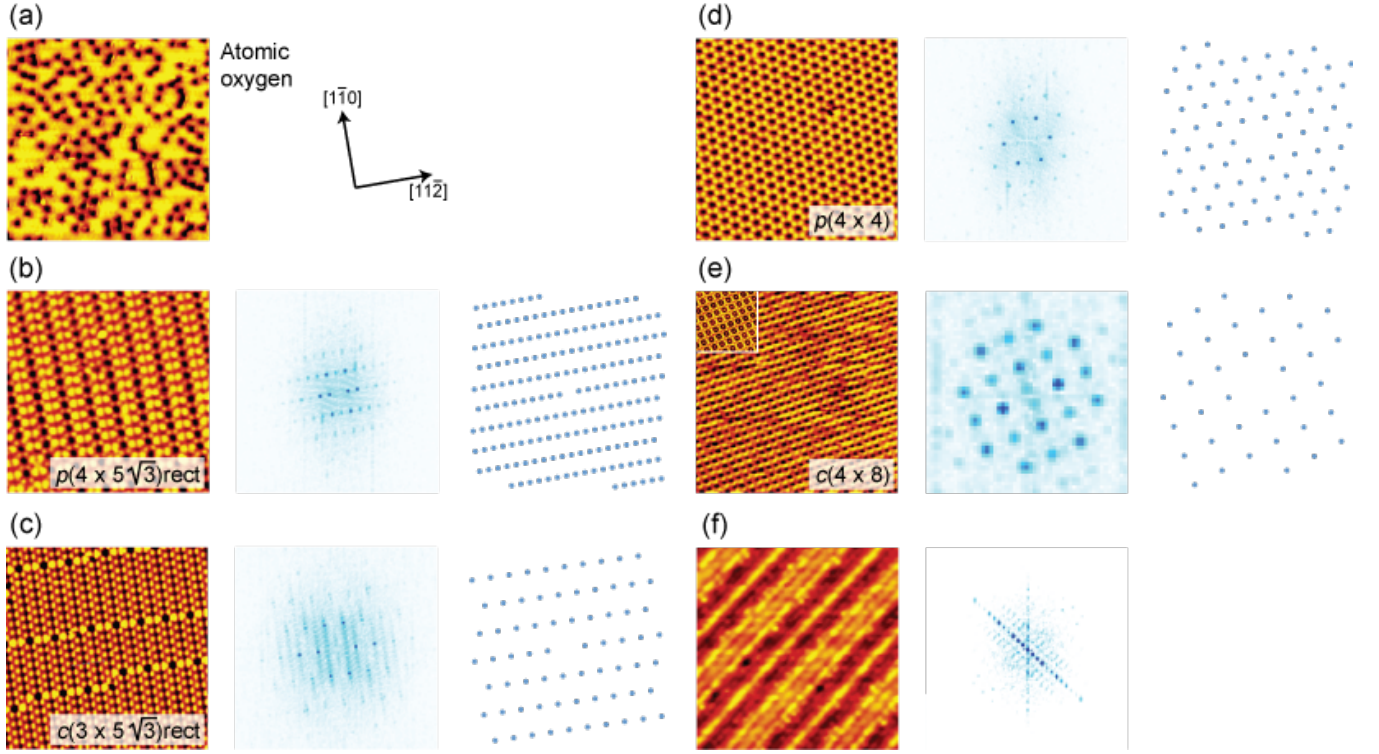


FIG. 1: (Color online) Phases of oxidized Ag(111) observed in the present study. Further phases observed previously are specified in Table I. The STM images to the left in the panels are supplemented by the FFTs of the STM images (middle parts of the panels) and by the theoretical LEED images simulated on the basis of the symmetry assignments (right-hand parts). The surface directions for all images are indicated in panel (a). (a) $70 \text{ \AA} \times 70 \text{ \AA}$, 1.12 nA, 9.8 mV. The depressions are interpreted as chemisorbed atomic oxygen with a coverage of approximately 11% of a monolayer. (b) $200 \text{ \AA} \times 200 \text{ \AA}$, 0.62 nA, 39.1 mV. $p(4 \times 5\sqrt{3})\text{rect}$. (c) $200 \text{ \AA} \times 200 \text{ \AA}$, -1.2 nA, -92.8 mV. $c(3 \times 5\sqrt{3})\text{rect}$. (d) $200 \text{ \AA} \times 200 \text{ \AA}$, 0.99 nA, 39.1 mV. $p(4 \times 4)$. (e) $200 \text{ \AA} \times 200 \text{ \AA}$, 0.64 nA, 110.5 mV. $c(4 \times 8)$. The inset shows the same surface phase measured with a different tip state. $60 \text{ \AA} \times 60 \text{ \AA}$, -0.34 nA, -109.6 mV. (f) $200 \text{ \AA} \times 200 \text{ \AA}$, 0.41 nA, 1250.0 mV. Striped structure.

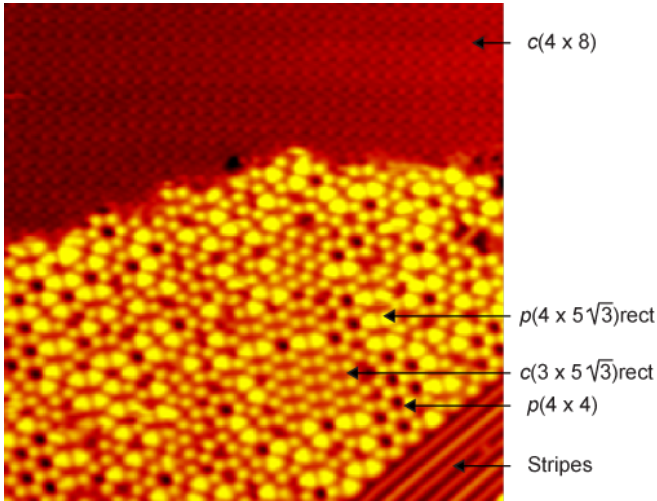


FIG. 2: (Color online) Coexistence of phases. $250 \text{ \AA} \times 250 \text{ \AA}$ STM image of a Ag(111) sample exposed to 5×10^{-8} Torr atomic oxygen for 40 min at 500 K sample temperature (-0.44 nA, -55.8 mV).

Here we present a detailed and thorough experimental and theoretical study of oxygen adsorption on Ag(111), with new data concerning both previously observed structures and hitherto new phases of oxidized Ag(111). The present study shows that the $p(4 \times 4)$ phase is embedded in a wider context of two additional phases, the $c(3 \times 5\sqrt{3})\text{rect}$ and $p(4 \times 5\sqrt{3})\text{rect}$ structures. It is also found that the $p(4 \times 4)$ structure, to our knowledge in contrast to the $c(3 \times 5\sqrt{3})\text{rect}$ and $p(4 \times 5\sqrt{3})\text{rect}$ phases, can host foreign atoms and molecules. Finally, the existence of two more phases with a $c(4 \times 8)$ and "stripe" character is reported.

II. EXPERIMENTAL AND THEORETICAL METHODS

The experiments were carried out in the STM laboratory and at the vacuum ultraviolet/soft x-ray synchrotron radiation facility ASTRID at Aarhus University. In the STM laboratory we used an ultra-high vacuum (UHV) chamber with a base pressure of 1×10^{-10}

Torr, equipped with standard instrumentation for sample cleaning, the Aarhus STM,⁶⁸ a low-energy electron diffractometer, and a thermal gas cracker from Oxford Instruments for atomic oxygen exposure with a cracking efficiency which in our experiments varied from 30% at 10^{-9} to 14% at 10^{-6} Torr total pressure. Directly connected to the UHV chamber is a small and compact high pressure cell which makes it possible to do molecular oxygen at pressures up to one atmosphere. After oxygen exposure the sample was characterized by STM and, in some cases, low-energy electron diffraction (LEED). The transfer between the high pressure cell and the UHV chamber could be accomplished within less than 15 min of oxygen exposure. Most of the STM experiments were performed at room temperature, although some of the STM images were recorded at liquid nitrogen temperature, which sometimes resulted in higher spatial resolution.

For the XPS measurements the surfaces were prepared and initially characterized in the STM chamber and then brought to the SX-700 beamline⁶⁹ of ASTRID in a vacuum suitcase with a base pressure better than 1×10^{-9} Torr. The pressure during transfer from the vacuum chambers to the suitcase, which could be accomplished within a minute, rose to in between 1×10^{-8} and 1×10^{-7} Torr. The base pressure of the UHV chamber of the SX-700 beamline is 1×10^{-10} Torr. After the XPS measurement the sample was transferred back to the STM chamber and the status of the sample reinvestigated by STM. The control experiments ensured that the examined structures were still present and clearly visible in the STM, although some minor deterioration of the surface might have occurred.

The Ag(111) surface was cleaned by repeated sputter/annealing cycles. It was then oxidized by exposing it to either atomic oxygen at partial atomic oxygen pressures of 1×10^{-9} to 1×10^{-6} Torr or molecular oxygen at pressures between 0.5 and 10 Torr. During oxygen exposure the Ag(111) sample was held at temperatures in between 420 and 600 K for an exposure time of 10 to 50 min. Following this recipe, the structure of the oxidized surface varied with oxygen pressure, sample temperature, and exposure time. Most often, the prepared surface exhibited co-existing domains of different surface phases. However, it was possible to prepare single phase surfaces for some of the structures presented below by carefully tuning the preparation parameters.

Bare *et al.*,⁹ have proposed an alternative preparation procedure, in which the surfaces is exposed to NO_2 at pressures between 5×10^{-8} to 5×10^{-6} Torr, while the sample is kept at the same temperatures as described above. This method has also been used in a variety of subsequent studies.^{11,12,43,63,70,71,72,73,74,75,76} Here we do not present any results obtained on samples prepared by this NO_2 method, although we did carry out a limited number of such studies. Consistent with Carlisle *et al.*,¹² we were able to produce the atomic oxygen, $p(4 \times 5\sqrt{3})\text{rect-O}$, and $p(4 \times 4)\text{-O}$ phases in these studies,

which indicates that the use of NO_2 instead of atomic or molecular oxygen does not significantly change the picture drawn up here.

All the density functional theory (DFT) calculations reported here were carried out with the Perdew-Burke-Ernzerhof generalized gradient approximation⁷⁷ in periodic supercells within the plane-wave pseudopotential formalism as implemented in the CASTEP code.⁷⁸ As discussed below, a variety of unit cells were used, all consisting of five layer Ag(111) slabs and with fine Monkhorst-Pack \mathbf{k} -point meshes equivalent to at least $24 \times 24 \times 1$ per (1×1) surface unit cell. During structure optimizations the top layer of Ag atoms as well as the oxide overlayer atoms were allowed to relax, whilst the bottom four layers of Ag were held fixed. From the DFT results simulated STM images were obtained using the simple Tersoff-Hamann approximation.⁷⁹ A “tip” height of 2.5 Å above the highest atom in each overlayer for occupied states within 2 eV of the Fermi level was used.

III. RESULTS AND DISCUSSION

A. Overview of the observed surface structures

Figure 1 displays STM images of all the phases which we have observed experimentally. The symmetry assignments ($c(3 \times 5\sqrt{3})\text{rect}$, $p(4 \times 5\sqrt{3})\text{rect}$, and $c(4 \times 8)$ for the hitherto non-assigned phases (see below for a more detailed description) were derived on the basis of the STM results. The middle parts of the panels represent the fast Fourier transform (FFT) of the STM images, while the right-hand parts reproduce LEED simulations obtained from the symmetry assignments provided on the basis of the STM observations. These LEED results are in excellent agreement with the FFTs, which lends further credibility to the STM-based symmetry assignments for the oxygen-induced phases.

At the lowest oxygen coverages an apparently disordered arrangement of depressions is observed in the constant current STM images (Fig. 1(a)). The depressions are interpreted as atomic oxygen adsorbates, consistent with previous studies¹² and the well-known fact that oxygen depletes the local density of states at the Fermi level, leading to a depression-like appearance of atomic oxygen on metal surfaces.⁸⁰ Domains of this disordered structure are also frequently observed to co-exist with domains of the structures shown in Figs. 1(b) to (d).

The structure in Fig. 1(b) was previously observed by Carlisle *et al.*¹² and was assigned to the decomposition of the $p(4 \times 4)$ structure in panel (d). The structure, which we briefly mentioned in a previous report,¹⁹ has a $p(4 \times 5\sqrt{3})\text{rect}$ unit cell in the convenient terminology for rectangular symmetries on hexagonal surfaces introduced by Biberian and van Hove.⁸² In matrix notation the unit cell (the conventional and primitive unit cells

TABLE I: Summary of the structures and preparation conditions for oxygen on Ag(111). For each preparation the first unequivocal identification (albeit not necessarily with the correct symmetry assignment and geometry) in literature is given. The asterisk indicates that the structure has been observed in the present study.

Structure	Atomic oxygen	Molecular oxygen	NO ₂
Atomic oxygen	$\times^{a,*}$	$\times^{b,*}$	$\times^{c,*}$
$p(\sqrt{3} \times \sqrt{3})\text{R}30^\circ$		\times^d	
$p(4 \times 5\sqrt{3})\text{rect}$	$\times^{e,*}$	$\times^{b,*}$	$\times^{c,*}$
$c(3 \times 5\sqrt{3})\text{rect}$	$\times^{e,*}$	$\times^{a,*}$	
$p(4 \times 4)$	$\times^{e,*}$	$\times^{f,*}$	$\times^{g,*}$
$c(4 \times 8)$	$\times^{a,*}$		
Striped structure	$\times^{a,*}$	$\times^{a,*}$	
$p(7 \times 7)$		\times^h	

^aPresent work.

^bReference 21.

^cReference 12.

^dA $p(\sqrt{3} \times \sqrt{3})\text{R}30^\circ$ overlayer was identified by Müller² on epitaxially grown Ag(111) films for relatively small oxygen exposures (100 L). Later results on the Ag(111) crystal, which show no formation of overlayers after oxygen exposure up to 3000 L under otherwise similar conditions, contradict these initial experiments.²² An overlayer with a $p(\sqrt{3} \times \sqrt{3})\text{R}30^\circ$ symmetry was once again reported by Bao *et al.* who used STM to study Ag samples exposed to pressures around one atmosphere^{32,36} (see also Ref. 81). In their first study,³² however, Bao *et al.* used facets of Ag single crystal spheres rather than a true Ag(111) single crystal. As already concluded by Engelhardt and Menzel²² terraces of limited width might behave qualitatively differently from extended single crystal surfaces and, therefore, the applicability of this study to Ag(111) single crystals is not obvious. In a subsequent study Bao *et al.*³⁶ then indeed used a Ag(111) single crystal and again reported STM observations of an overlayer with a $p(\sqrt{3} \times \sqrt{3})\text{R}30^\circ$ symmetry.

^eReference 19.

^fReference 5.

^gReference 9.

^hReference 42.

are identical) is described by

$$\begin{pmatrix} 10 & 5 \\ 0 & 4 \end{pmatrix}.$$

The structure in Fig. 1(c) also possesses a rectangular symmetry with a conventional unit cell of $c(3 \times 5\sqrt{3})\text{rect}$ symmetry. The brighter lines from left to right are units of the $p(4 \times 5\sqrt{3})\text{rect}$ structure. We have observed that domains of the $c(3 \times 5\sqrt{3})\text{rect}$ structure always contain at least small fractions of defects of $p(4 \times 5\sqrt{3})\text{rect}$ symmetry, which in room temperature experiments sometimes have been observed to move along the $[1\bar{1}0]$ direction. The primitive unit cell of the $c(3 \times 5\sqrt{3})\text{rect}$ phase is given by⁸³

$$\begin{pmatrix} 3 & 0 \\ -4 & 5 \end{pmatrix}.$$

Panel (d) of Fig. 1 shows the well-known $p(4 \times 4)$ structure, which has been the subject of surface science investigations since the early 1970s, whereas the structures in panels (e) and (f) are reported here for the first time. The first of these has a $c(4 \times 8)$ symmetry, while the appearance of the second structure is characterized by stripes of variable thickness along the $\{1\bar{1}0\}$ surface directions. In matrix notation the primitive unit cell of the $c(4 \times 8)$ structure is given by

$$\begin{pmatrix} 3 & 2 \\ -1 & -2 \end{pmatrix}.$$

Table I summarizes the conditions, which here and in other studies have been used to prepare the different surface structures. Both the atomic and molecular oxygen recipes are very versatile in terms of the variety of structures which can be produced. The NO₂ recipe has so far primarily been used to prepare oxidized Ag(111) surfaces covered entirely by the $p(4 \times 4)$ structure.^{9,11,12,20,43} The present results show that also the $p(4 \times 5\sqrt{3})\text{rect}$ structure can be produced by exposing the Ag(111) crystal to NO₂. Due to the similarity of the $p(4 \times 4)$, $p(4 \times 5\sqrt{3})\text{rect}$, and $c(3 \times 5\sqrt{3})\text{rect}$ structures (see below) it can be expected that it also is possible to form the latter using NO₂, while it is more difficult to draw conclusions along these lines regarding the remaining structures.

For most preparation conditions a variety of co-existing surface structures appear. This is illustrated in Fig. 2, which displays an STM image recorded after exposing the surface to 5×10^{-8} Torr atomic oxygen at 500 K for 40 min. In this STM image the $p(4 \times 5\sqrt{3})\text{rect}$, $c(3 \times 5\sqrt{3})\text{rect}$, $p(4 \times 4)$, $c(4 \times 8)$, and stripe structures are found to co-exist within a $250 \text{ \AA} \times 250 \text{ \AA}$ area of the surface. It is observed that the $p(4 \times 5\sqrt{3})\text{rect}$, $c(3 \times 5\sqrt{3})\text{rect}$, and $p(4 \times 4)$ structures have very similar STM appearances with respect to their height profiles (brightness), whereas the STM height profile for the $c(4 \times 8)$ structure is much lower. As will be seen and discussed in further detail below this reflects that the atomic geometries of the $p(4 \times 5\sqrt{3})\text{rect}$, $c(3 \times 5\sqrt{3})\text{rect}$, and $p(4 \times 4)$ structures are indeed very similar.

B. Ag₆/Ag₁₀ building block structures

The STM images of the $p(4 \times 5\sqrt{3})\text{rect}$, $c(3 \times 5\sqrt{3})\text{rect}$, and $p(4 \times 4)$ phases in Figs. 1(b-d) are characterized by ordered arrays of unresolved bright features. Higher resolution images are depicted in Figs. 3(a), (c), and (e). From these it is seen that the bright features contain atomic sub-structure. In the case of the $c(3 \times 5\sqrt{3})\text{rect}$ phase a particular tip state even allowed all Ag atoms in the overlayer to be resolved (inset of panel (c)). For the $c(3 \times 5\sqrt{3})\text{rect}$ and $p(4 \times 4)$ phases the arrangement of the silver and oxygen atoms has already been discussed in detail in Ref. 19. In brief, both structures are built from close-to identical elements of Ag₆ triangles with the

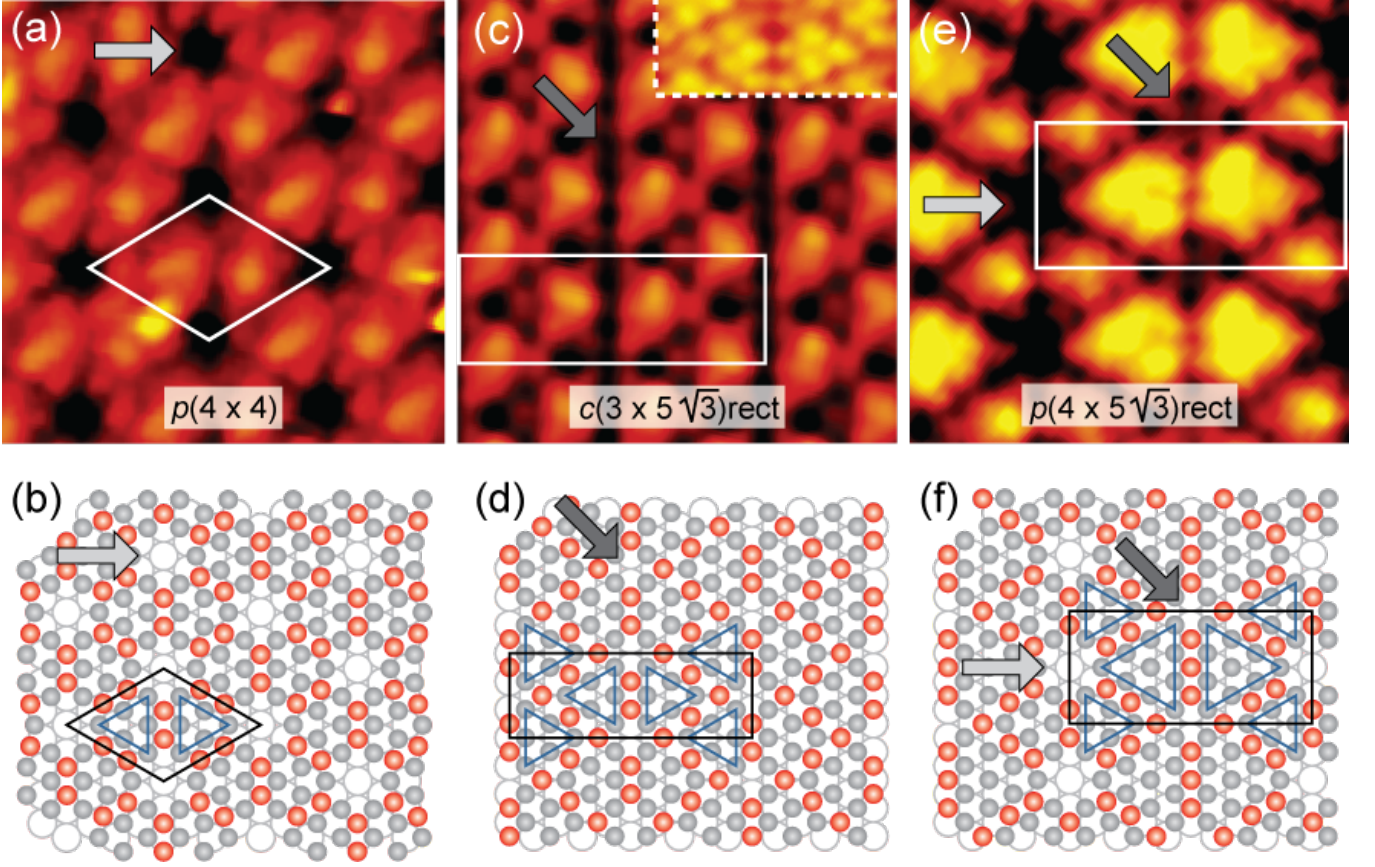


FIG. 3: (Color online) (a), (c), (e) STM images and (b), (d), (f) experimentally derived structures of the $\text{Ag}_6/\text{Ag}_{10}$ building block structures. The structural models for the $p(4 \times 4)$ and $c(3 \times 5\sqrt{3})\text{rect}$ phases in panels (b) and (d) also contain the in Ref. 19 theoretically derived positions of the oxygen atoms. The red/dark gray spheres represent the oxygen, (medium) gray the overlayer silver, and the open spheres the $\text{Ag}(111)$ substrate atoms. The blue lines are guides for the eye indicating the Ag_6 and Ag_{10} building blocks. (a) $35 \text{ \AA} \times 35 \text{ \AA}$, -0.42 nA , -21.7 mV . $p(4 \times 4)$. (b) $35 \text{ \AA} \times 35 \text{ \AA}$, -0.40 nA , -34.2 mV . $c(3 \times 5\sqrt{3})\text{rect}$. (c) $35 \text{ \AA} \times 35 \text{ \AA}$, -0.38 nA , -17.4 mV . $(4 \times 5\sqrt{3})\text{rect}$. The inset in panel (c) shows a highly resolved Ag_6 dimer with all 12 Ag atoms visible (-0.42 nA , -21.7 mV). The light (dark) arrows mark the voids characteristic for the $p(4 \times 4)$ ($c(3 \times 5\sqrt{3})\text{rect}$ -like) phase. Both types of voids are found in the $p(4 \times 5\sqrt{3})\text{rect}$ structure.

Ag atoms of a single Ag_6 all located either in fcc or hcp sites. Each unit cell contains one fcc triangle and one hcp triangle. The site difference implies a slight asymmetry between the two triangles of a dimer, which, at least for the $p(4 \times 4)$ phase, is further enhanced by small rotations in converse directions for the fcc and hcp triangles.^{20,43} Indeed, for certain tip states fcc triangles and hcp triangles are imaged differently in STM, as is illustrated in Figure 5(a-b). On the basis of the STM measurements we thus propose the structural models depicted in Figures 3(b) and (d). It is difficult to provide a detailed assignment for the location of the oxygen atoms, which normally are not visible in STM due to the depletion of the local density of states at the Fermi level typical for oxygen (see, however, below for an example in which some oxygen density is visible). For the $c(3 \times 5\sqrt{3})\text{rect}$ and $p(4 \times 4)$ phases the oxygen atom positions were derived by evaluating a large variety of different structures in DFT calculations.^{19,20} The positions of the oxygen

atoms in the thus derived structural models have been included in the models shown in Fig. 3(b) and (d), which were suggested on the basis of the experimental STM results. Figures 4(a) and (b) show the structural models emerging from the calculations. The corresponding STM simulations in panels (d) and (e) are found to be in good agreement with the experimental STM results in Figure 3(a) and (c). The DFT adsorption energies (eV/O) are provided in Table II. They are seen to be the same to within the uncertainty of the DFT results.

The arrangement of the Ag atoms in the $p(4 \times 5\sqrt{3})\text{rect}$ structure in Figure 3(e) can be understood from an extension of the Ag_6 building block model for the $c(3 \times 5\sqrt{3})\text{rect}$ and $p(4 \times 4)$ phases. The larger triangles constitute an additional Ag_{10} building block, which typically appears in dimer form, again with half of the silver atoms in fcc and the other half in hcp sites. In the pure $p(4 \times 5\sqrt{3})\text{rect}$ phase the Ag_6 and Ag_{10} dimers are then arranged as depicted in Fig. 3(f). It is noteworthy

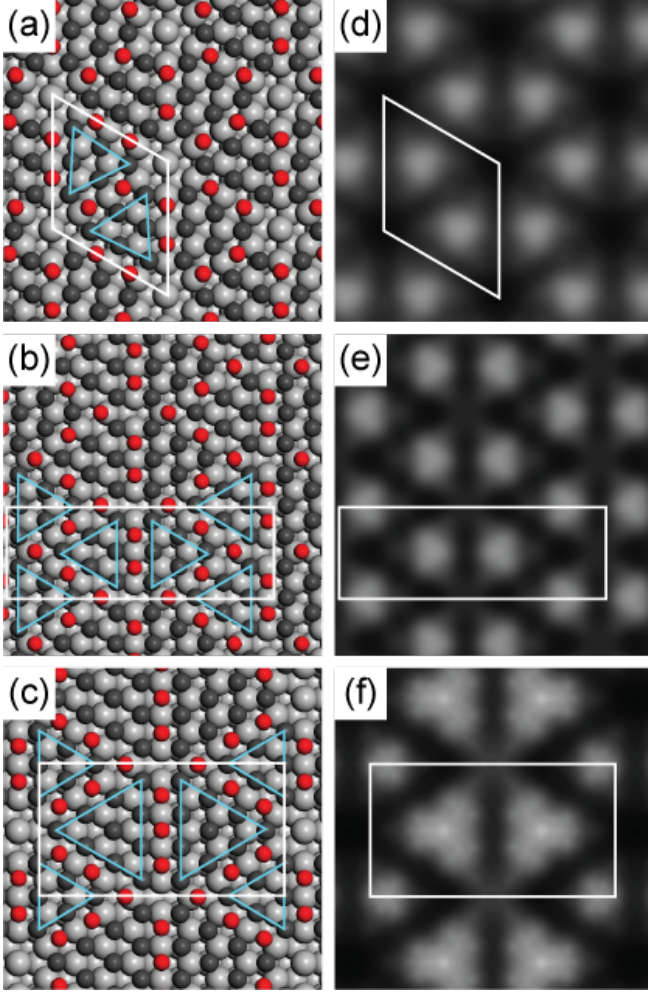


FIG. 4: (Color online) (a) to (c) Final geometrical models of the building block structures $p(4 \times 4)$, $c(3 \times 5\sqrt{3})$ rect, and $p(4 \times 5\sqrt{3})$ rect. (d) to (f) Tersoff-Hamann simulations of the structures in (a) to (c). The dark (light) gray spheres represent Ag atoms in the overlayer (substrate) and the red spheres O atoms. The blue lines are guides for the eye indicating the Ag₆ and Ag₁₀ building blocks.

thy that the $p(4 \times 5\sqrt{3})$ rect structure appears as a mixture of the $p(4 \times 4)$ and $c(3 \times 5\sqrt{3})$ rect overlayers, with the voids between four Ag₁₀ and two Ag₆ triangles being $c(3 \times 5\sqrt{3})$ rect-like (dark arrow in Fig. 3(f)) and those between four Ag₆ and two Ag₁₀ being $p(4 \times 4)$ -like (light arrow).

As in the cases of the $p(4 \times 4)$ and $c(3 \times 5\sqrt{3})$ rect phases discussed above the oxygen atoms incorporated into the $p(4 \times 5\sqrt{3})$ rect structure are normally not visible in STM. Again, we carried out DFT calculations for a large number of different arrangements of both oxygen and silver atoms to find the most stable arrangement of surface atoms. This search also included geometries which deviated from the experimentally derived Ag₆/Ag₁₀ building block structure. Among the investigated structures, the

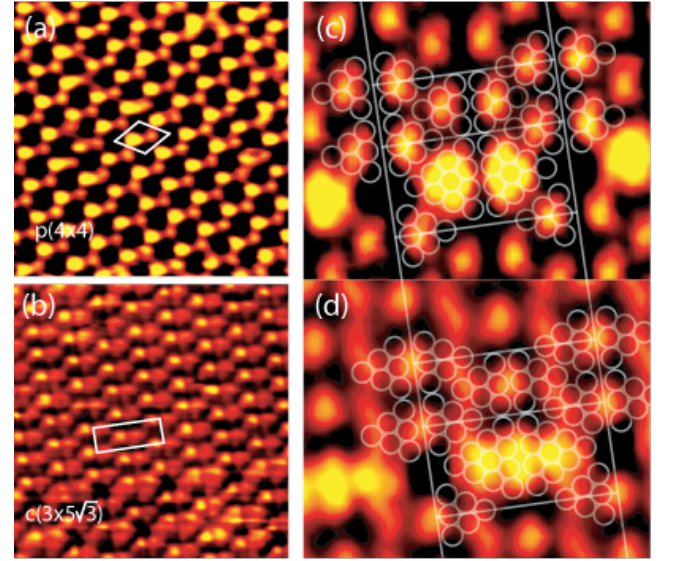


FIG. 5: (Color online) Building block structures imaged with special tip states. (a) and (b) Imaging conditions which let the hcp and fcc Ag₆ triangles appear differently. (a) $100 \times 100 \text{ \AA}^2$, 0.54 nA, 9.8 mV. (b) $100 \times 100 \text{ \AA}^2$, 0.85 nA, 55 mV. (c) and (d) Images of the same area in (c) normal imaging mode and (d) oxygen imaging mode. $47 \times 37 \text{ \AA}^2$. (c) 1.48 nA, 55 mV. (d) 1.49 nA, 55 mV.

one displayed in Figure 3(f) was found to be the most stable one. The model is indeed based on the two different building blocks suggested above on the basis of the STM results. The oxygen atoms reside in the same sites as for the $p(4 \times 4)$ and $c(3 \times 5\sqrt{3})$ rect phases, a finding which lends further credibility to the proposed model. The DFT oxygen adsorption energy (eV/O) (cf. Table II) is seen to be the same, to within the DFT uncertainty, as that of the other two Ag₆ building block structures.

Fig. 4 contains the final structural models for all three Ag₆/Ag₁₀ phases in panels (a)-(c). The Figure also shows that the Tersoff-Hamann (TH) STM simulations are in good agreement with the STM results. In particular, the TH STM simulations reproduce the experimentally observed high apparent height of the silver atoms in the centers of the Ag₆/Ag₁₀ triangles, which are characterized by a high silver coordination. The lower-Ag-coordinated edge atoms and even more so the corner atoms of the Ag triangles have a much lower local density of states intensity and therefore appear lower than the triangle center atoms. We also note that by slightly modifying the simulated tip apex height and bias conditions we are not only able to reproduce the experimentally observed triangular appearance of the building blocks shown in Figs. 4(d-f), but also the more spherical appearance of the bright features in Fig. 1(b-d).

In Table II we compare the stoichiometries and top layer silver and oxygen atom densities of the three Ag₆/Ag₁₀ building block structures. Both the $p(4 \times 4)$

and $c(3 \times 5\sqrt{3})$ rect phases have a Ag_2O stoichiometry, but the $c(3 \times 5\sqrt{3})$ rect has slightly higher Ag and O atom densities than the $p(4 \times 4)$. Judging from the stoichiometry the $p(4 \times 5\sqrt{3})$ rect phase seems to be more oxygen-deficient; however, the absolute oxygen density is the same for the $p(4 \times 4)$ and $p(4 \times 5\sqrt{3})$ rect structures, while the Ag density is increased for the $p(4 \times 5\sqrt{3})$ rect and reaches the same level as in the $c(3 \times 5\sqrt{3})$ rect. It is thus not correct to view the $p(4 \times 5\sqrt{3})$ rect phase as a decomposition phase of the $p(4 \times 4)$, as suggested by Carlisle *et al.*¹² While this characterization applies to the $p(4 \times 5\sqrt{3})$ rect in relationship to the $c(3 \times 5\sqrt{3})$ rect phase, the $p(4 \times 5\sqrt{3})$ rect structures rather corresponds to a Ag-rich reconstruction of the $p(4 \times 4)$ structure.

From the similar geometrical arrangements of the silver and oxygen atoms in the three $\text{Ag}_6/\text{Ag}_{10}$ building block structures as revealed in the STM images it seems likely that the electronic and chemical characteristics of these phases should be very similar. This is corroborated by the O 1s x-ray photoelectron spectra depicted in Fig. 6. Within the measuremental uncertainty of 0.1 eV the O 1s binding energies are the same for all three structures (528.5 eV) and they agree quite well with previous measurements on the $p(4 \times 4)$ phase⁸ (528.1 eV), although they are about 0.4 eV higher in energy (they are more similar to the recent measurement by Reichelt *et al.*,²¹ who report a binding energy of 528.3 eV). However, the O 1s peak observed for the $p(4 \times 4)$ phase prepared from atomic oxygen is located at 528.7 eV, and this upwards shift in energy we cannot explain at present. It is further noted that all spectra contain a high energy component at energies between 530.1 and 530.5 eV. This peak is particularly pronounced for the $p(4 \times 4)$ phase prepared using molecular oxygen, i.e., at an elevated pressure. Previously it has been assigned to both carbonates and a reactive oxygen species.^{10,21} Considering that contaminations released from the reactor walls are common in high pressure experiments such as used in the molecular oxygen preparation of the $p(4 \times 4)$ phase (10 Torr in the present case) it seems most likely that the peak is related to carbonates.

Finally it is noted, that it is sometimes possible to directly image some of the surface oxygen density in the STM images (see, e.g., also Ref. 84). As stated above, for normal STM tunneling conditions oxygen adsorbed on Ag is not easily identified in the STM images, but, as demonstrated in Figure 5(d) for a mixed $c(3 \times \sqrt{5})$ rect/ $p(4 \times \sqrt{5})$ rect surface, rare tip states seem to enhance those oxygen atoms which are coordinated by four top layer silver atoms. The oxygen atoms are identified from a comparison to the STM image in normal imaging mode in Figure 5(c) and the structural models in Figure 3(d-f). In this special tip state image the silver atoms of the smaller Ag_6 are not imaged at all, while the centers of the Ag_{10} appear nearly as bright as the fourfold-coordinated oxygen atoms. The threefold-coordinated oxygens, however, remain invisible even for the special tip state.

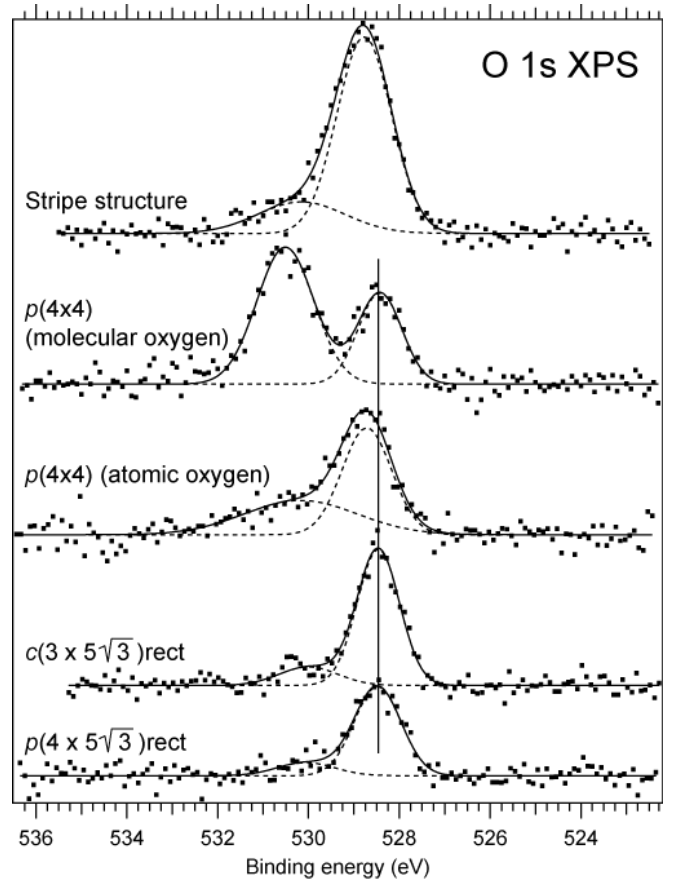


FIG. 6: O 1s x-ray photoelectron spectra of the indicated preparations. The specifications "molecular oxygen" and "atomic oxygen" refer to which preparation method was used (cf. Table I).

C. The $p(4 \times 4)$ phase as a host-guest structure

In Figure 7 STM images of the $p(4 \times 4)$ phase are shown, which were recorded at varying bias voltages. As shown in panel (a), at the lowest biases of approximately -15 meV the STM image exhibits the typical honeycomb appearance with the structural voids displayed as depressions (cf. the atomic model in Fig. 3(a)). When the bias is increased to about -1000 mV a fraction of the voids appears filled (panel (b)). At the highest biases used, around -2000 mV, the fillings already visible at the intermediate bias are now the brightest features in the STM image, while other voids display fillings with a smaller apparent height in the image. Only a very minor fraction of voids seem to be unfilled.

We frequently observed the presence of fillings in the voids of the $p(4 \times 4)$ structure. The fillings are most easily imaged at elevated biases of both tunneling polarities, and they occur in preparations from both atomic and molecular oxygen. Whether they exist for preparations from NO_2 cannot be clarified here, since we used either atomic or molecular oxygen for the preparation of

TABLE II: Stoichiometry, top layer Ag and O atom densities, and DFT adsorption energies E_{ads} of the here described O/Ag overlayers. The data for the $c(4 \times 8)$ structure are tentative, since the geometry model presented in the text so far has not been confirmed by further experimental and/or theoretical methods. E_{ads} is defined as in Reference 1.

	Stoichiometry	Ag density	O density	E_{ads} (eV/O)
$p(4 \times 4)$	Ag_2O	0.104 \AA^{-2} (0.75 ML)	0.052 \AA^{-2} (0.375 ML)	0.46
$c(3 \times 5\sqrt{3})\text{rect}$	Ag_2O	0.111 \AA^{-2} (0.80 ML)	0.055 \AA^{-2} (0.40 ML)	0.39
$p(4 \times 5\sqrt{3})\text{rect}$	$\text{Ag}_2\text{O}_{0.94}$	0.111 \AA^{-2} (0.80 ML)	0.052 \AA^{-2} (0.375 ML)	0.42
$c(4 \times 8)$	$\text{Ag}_2\text{O}_{1.6}$	0.043 \AA^{-2} (0.31 ML)	0.035 \AA^{-2} (0.25 ML)	

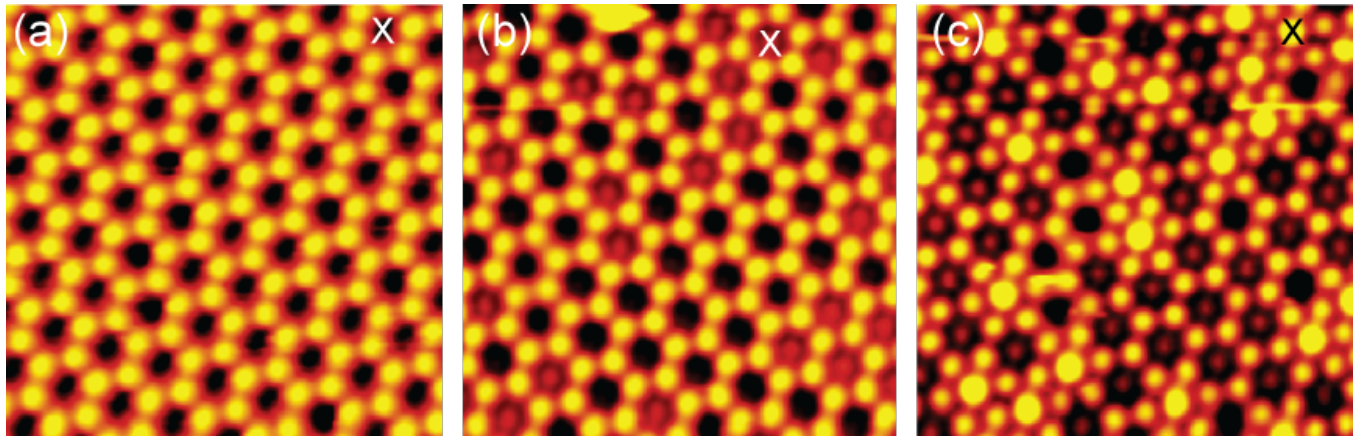


FIG. 7: (Color online) The $p(4 \times 4)$ phase as a host-guest architecture. The images were recorded on a sample prepared using atomic oxygen. (a) $90 \text{ \AA} \times 90 \text{ \AA}$, -0.35 nA , -15.9 mV . (b) $90 \text{ \AA} \times 90 \text{ \AA}$, -0.43 nA , -1030.3 mV . (c) $90 \text{ \AA} \times 90 \text{ \AA}$, -0.44 nA , -2024.2 mV . (a) and (c) were recorded at the same time (forward and backwards movements of the tip). (b) was recorded immediately prior to (a) and (c), and it was also accompanied by a simultaneous recording at low bias (-33 V). The latter image showed the same characteristics as the image in panel (a). The sample positions differ slightly between (a)/(c) and (b) due to thermal drift; the spatial relationship can, however, be inferred from the pattern of the hexagon fillings. Identical absolute positions have been marked by a cross.

the surfaces investigated by STM. Interestingly, we have not seen any such filling for the $p(4 \times 5\sqrt{3})\text{rect}$ phase, although it – in contrast to the $c(3 \times 5\sqrt{3})\text{rect}$ structure – contains the same kind of voids as visible from the structural models in Fig. 3.

We suggest that the fillings are related to adsorbate species in the voids of the $p(4 \times 4)$ phase. Since we observed such fillings both directly after preparation of the surface by either atomic or molecular oxygen as well as after measurements for a time span of several hours, it seems unlikely that rest gas contamination can be made responsible for the fillings. Nonetheless, at present we cannot specify the chemical nature of the fillings and we can just note that the observation of the fillings suggests an interesting host-guest character of the $p(4 \times 4)$ phase, which would deserve a more systematic study.

D. The $c(4 \times 8)$ and stripe structure

Finally we would like to discuss two additional structures not observed previously. These are the $c(4 \times 8)$ and stripe phases of Figure 1(e-f). In both cases it is difficult to provide the exact details of the atomic scale structures. The reasons are that for the $c(4 \times 8)$ structure we have so far have not been able to find a recipe for preparing a single phase $c(4 \times 8)$ surface, and for the stripe structure there exists a larger manifold of similar, co-existing structures. The difficulty in preparing surfaces covered by a single coherent structure have prevented the use of averaging techniques such as LEED or XPS, which would have resulted in useful chemical and structural information. In the following we therefore limit ourselves to primarily describing the characteristics of the structures to the extent they could be extracted from the STM data.

Starting with the $c(4 \times 8)$ structure, its symmetry assignment was derived from comparing its unit cell with those of other phases appearing in the same STM image.

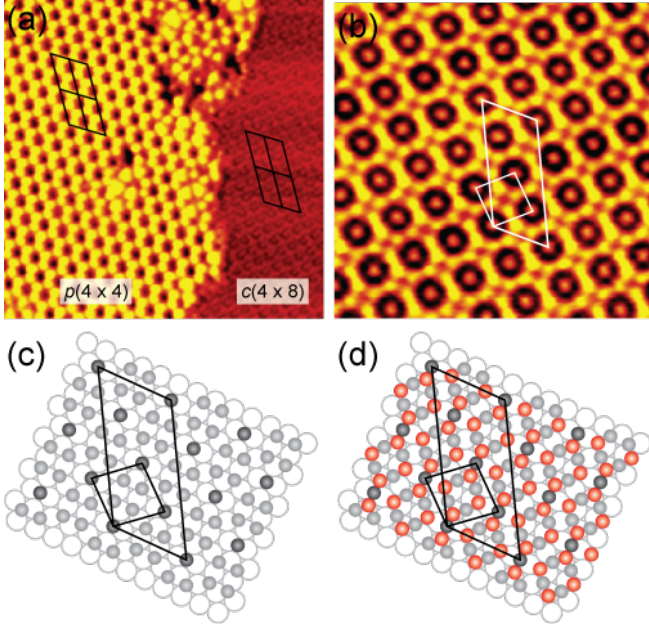


FIG. 8: (Color online) STM images and geometrical models of the $c(4 \times 8)$ phase. The colors are as in Figure 3, with the addition that the darkest gray sphere represent the Ag atoms which appear isolated in the STM images. (a) $200 \text{ \AA} \times 200 \text{ \AA}$, -0.40 nA , -185.8 mV . The $c(4 \times 8)$ is here found to occur simultaneously with the $p(4 \times 4)$ phase. The large parallelograms depict arrays of four conventional unit cells of the $c(4 \times 8)$ structure. The superposition of the parallelogram onto the $p(4 \times 4)$ phase confirms the (4×8) assignment, since each unit cell is seen to comprise two $p(4 \times 4)$ unit cells. (b) $60 \text{ \AA} \times 60 \text{ \AA}$, -0.34 nV , -109.6 mV . (c) Tentative geometry of the Ag atoms in the $p(4 \times 8)$ structure. The parallelograms in (b) to (d) show both the conventional and primitive unit cells.

Such a comparison is shown in Fig. 8(a). The correctness of the assignment is supported by the good agreement between the LEED simulation based on the $c(4 \times 8)$ unit cell in Figure 1(e). Since oxygen typically is invisible in the STM images it is assumed that the bright features in the more highly resolved STM images of the $c(4 \times 8)$ structure correspond to silver atoms, cf. Fig. 8(b). This assignment leads us to suggest the tentative top layer Ag atom geometry depicted in Fig. 8(c). It is the only geometry for which the bright features in the experimental image can be brought into coincidence with lattice sites. In this model, 20% of the top layer silver atoms reside in bridging sites, while the remaining silver atoms are found in both hcp and fcc hollow sites.

The ring-formed depressions around the Ag atoms in bridging sites indicate that the Ag atoms are surrounded by oxygen atoms. The placement of four oxygen atoms in the dark ring leads to the detailed geometry shown in Figure 8(d). In this geometry the coordination of the silver atoms by other top layer silver atoms is much lower than in the building block structures described in section

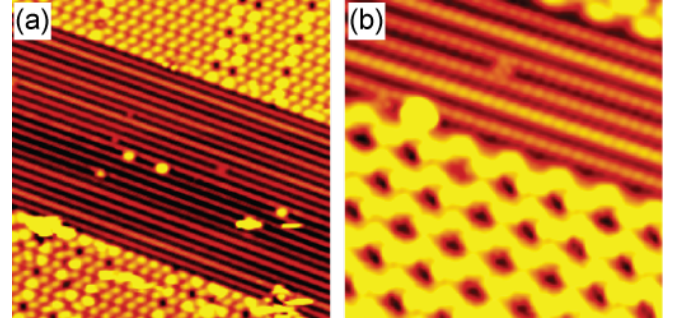


FIG. 9: (Color online) STM images of the stripe phase. (a) $200 \text{ \AA} \times 200 \text{ \AA}$, -0.41 nA , -25.0 mV . (b) $75 \text{ \AA} \times 75 \text{ \AA}$, -0.47 nA , 58 mV .

IIIB. In these structures silver atoms with a low silver coordination such as the corner atoms of the $\text{Ag}_6/\text{Ag}_{10}$ triangles were imaged with a reduced apparent height as compared to the fully silver-coordinated silver atoms in the centers of the triangles. As seen clearly in Figure 8(a), also the $c(4 \times 8)$ phase is characterized by a much smaller apparent height than the brightest features of the $p(4 \times 4)$ phase. We take this as an indication that the $c(4 \times 8)$ structures indeed is more highly oxidized than any of the building block structures.

The suggested structure for the $c(4 \times 8)$ possesses a Ag_5O_4 ($\text{Ag}_2\text{O}_{1.6}$) stoichiometry (cf. Table II). A very similar structure was observed previously for a Pd_5O_4 surface oxide.⁸⁵ A major difference between the present and the Pd oxide case is, however, the full commensurability of the Ag_5O_4 unit cell, while the Pd_5O_4 is incommensurate in one surface direction. It is seen that the proposed stoichiometry for the $c(4 \times 8)$ is more reminiscent of AgO than Ag_2O and that the density of Ag and O atoms is much lower in the $c(4 \times 8)$ as compared to the $\text{Ag}_6/\text{Ag}_{10}$ building block structures. This difference in stoichiometry and Ag and O densities in comparison to the $p(4 \times 4)$, $c(3 \times 5\sqrt{3})$, and $p(4 \times 5\sqrt{3})$ phases is surprising in view of the coexistence of these structures such as those in Figure 2. At present we cannot satisfactorily explain this finding.

Now turning to the stripe phase, we would first like to again emphasize that there exists a larger number of coexisting structures which appear as stripes in the STM measurements. Probably these structures have similar, but not exactly equal atomic geometries. That the geometries indeed differ between different domains of the stripe phase is quite obvious from a comparison of the displayed domains in Figs. 1(f) and 9. The common denominator of the domains is the occurrence of stripes along $\{1\bar{1}0\}$, but the arrangement and apparent height of the stripes are not always the same.

While it was difficult in general to obtain high resolution STM images on extended domains of stripe character, this was sometimes possible on smaller domains embedded in other structures. Figure 9 provides exam-

ples of such high-resolution STM images. We tentatively assume that the protruding features of these images are silver atoms. Along the $\{110\}$ directions the distance between these features corresponds to the Ag(111) nearest-neighbor distance $b = 2.89$ Å. In the perpendicular direction the distances of the rows is, however, not a multiple of $\sqrt{3}b$, as might have been expected. By comparison to the surrounding surface covered by domains of the $p(4 \times 4)$, $c(3 \times 5\sqrt{3})$ rect, and $p(4 \times 5\sqrt{3})$ rect phases it is estimated that the repetitive unit rather comprises four stripes and that this unit has a width of $4\sqrt{3}b$. In such a unit cell it is not possible to place all the silver atoms in the same lattice site. The differing brightness of adjacent stripes supports this conclusion.

The position of the oxygen atoms in the stripe phase cannot be specified in any detail from an analysis of the STM results. It seems likely that oxygen atoms reside in between the bright stripes. The XPS data in Figure 6 indicate that the oxygen content is considerably higher than in the $p(4 \times 4)$ and $c(3 \times 5\sqrt{3})$ rect phases. Similar to the $c(4 \times 8)$ structure and the corner atoms of the triangles in the building block structures, the stripes are imaged at a smaller apparent height compared to that of the adjacent domains of primarily $c(3 \times 5\sqrt{3})$ rect symmetry in panel (a) of Figure 9 and primarily $p(4 \times 4)$ in panel (b). This suggests that the silver coordination of the Ag atoms of the stripe phase is smaller than that of the Ag atoms in the centers of the triangles of the building block structures, which indicates a higher oxygen coordination and thus a higher oxygen content of the stripe phase. However, at present, we refrain from a more quantitative analysis, partly since it is unclear to what extent the XPS data represent fully covered surfaces and partly since the STM data cannot provide any more detailed information. It is noted, though, that metal/oxygen structure with quite a high oxygen content and exhibiting a stripe appearance have been observed on other metal surfaces such as Pt(110).⁸⁶

IV. CONCLUSIONS

We have shown from an interplay of STM and XPS experiments and DFT calculations that the oxidation of the Ag(111) surface may be structurally more complex than previously anticipated. Depending on the preparation conditions – oxidation agent, dose, and pressure, exposure time, and sample temperature during and af-

ter exposure – a large variety of different structures are found, essentially all of which may coexist. Among these phases we have identified a number of structures, which are formed from Ag₆/Ag₁₀ fundamental building blocks. This group of structures comprises both the renowned $p(4 \times 4)$ surface as well as two phases of $c(3 \times 5\sqrt{3})$ rect and $p(4 \times 5\sqrt{3})$ rect symmetry. The $p(4 \times 5\sqrt{3})$ rect structure had been observed previously,¹² but we have devised a new structural model which is in line with the geometries for the $p(4 \times 4)$ (Refs. 19 and 20) and $c(3 \times 5\sqrt{3})$ rect phases (Ref. 19) proposed recently and discussed in more detail here. In addition, we have observed two additional structures of $c(4 \times 8)$ and stripe character.

The present results suggest that a complex coexistence of oxide and oxygen adsorbate overlayers with varying contents of oxygen may form under the conditions of industrial oxidation catalysis. This is in contrast to the prevalent perception that the $p(4 \times 4)$ phase alone represents an adequate model for the surface under such conditions. It is conceivable that the complexity of the phase diagram has a profound influence on the dynamics of the catalytic process. Hence, although an increased understanding of the structure of the oxidized silver surface is presently being obtained as demonstrated in this and other studies,^{19,20,21,42,43,63} we are still far from a detailed understanding of the oxidized silver surface under reaction conditions. It appears likely that the structure of the silver oxide surface may vary in response to changes in the gas composition and the chemical potential of the reaction intermediates.

Acknowledgments

The competent assistance of the staff of the mechanical workshop of the Department of Physics and Astronomy in Aarhus is gratefully acknowledged. JS wishes to thank the European Commission for funding through a Marie Curie Intra-European Fellowship. AM is grateful to the Alexander von Humboldt foundation for partial support of this work and the European Science Foundation and EPSRC for a European Young Investigator Award (EURYI). Some of the calculations performed here were made possible by AM's membership of the UK's HPC Materials Chemistry Consortium, which is funded by EPSRC (EP/F067496).

* Electronic address: joachim.schnadt@sljus.lu.se

† Electronic address: fbe@inano.dk

¹ A. Michaelides, K. Reuter, and M. Scheffler, *J. Vac. Sci. Technol. A* **23**, 1487 (2005).

² K. Müller, *Z. Phys.* **195**, 105 (1966).

³ R. Dégeilh, *Vide* **139**, 29 (1969).

⁴ A. W. Deydari and C. H. N. Mee, *Phys. Status Solidi A*

17, 247 (1973).

⁵ G. Rovida, F. Pratesi, M. Maglietta, and E. Ferroni, *J. Vac. Sci. Technol.* **9**, 796 (1972).

⁶ G. Rovida, F. Pratesi, M. Maglietta, and E. Ferroni, *Surf. Sci.* **43**, 230 (1974).

⁷ H. Albers, W. J. J. van der Wal, and G. A. Bootsma, *Surf. Sci.* **68**, 47 (1977).

- ⁸ C. T. Campbell, *Surf. Sci.* **157**, 43 (1985).
- ⁹ S. R. Bare, K. Griffiths, W. N. Lennard, and H. T. Tang, *Surf. Sci.* **342**, 185 (1995).
- ¹⁰ V. I. Bukhtiyarov, V. V. Kaichev, and I. P. Prosvirin, *J. Chem. Phys.* **111**, 2169 (1999).
- ¹¹ C. I. Carlisle, D. A. King, M.-L. Bocquet, J. Cerdá, and P. Sautet, *Phys. Rev. Lett.* **84**, 3899 (2000).
- ¹² C. I. Carlisle, T. Fujimoto, W. S. Sim, and D. A. King, *Surf. Sci.* **470**, 15 (2000).
- ¹³ W.-X. Li, C. Stampfl, and M. Scheffler, *Phys. Rev. B* **67**, 045408 (2003).
- ¹⁴ W.-X. Li, C. Stampfl, and M. Scheffler, *Phys. Rev. B* **68**, 165412 (2003).
- ¹⁵ W.-X. Li, C. Stampfl, and M. Scheffler, *Phys. Rev. Lett.* **90**, 256102 (2003).
- ¹⁶ A. Michaelides, M.-L. Bocquet, P. Sautet, A. Alavi, and D. A. King, *Chem. Phys. Lett.* **367**, 344 (2003).
- ¹⁷ M.-L. Bocquet, A. Michaelides, D. Loffreda, P. Sautet, A. Alavi, and D. A. King, *J. Am. Chem. Soc.* **125**, 5620 (2003).
- ¹⁸ M.-L. Bocquet, A. Michaelides, P. Sautet, and D. A. King, *Phys. Rev. B* **68**, 075413 (2003).
- ¹⁹ J. Schnadt, A. Michaelides, J. Knudsen, R. T. Vang, K. Reuter, E. Lægsgaard, M. Scheffler, and F. Besenbacher, *Phys. Rev. Lett.* **96**, 146101 (2006).
- ²⁰ M. Schmid, A. Reicho, A. Stierle, I. Costina, J. Klikovits, P. Kostelnik, O. Dubay, G. Kresse, J. Gustafson, E. Lundgren, et al., *Phys. Rev. Lett.* **96**, 146102 (2006).
- ²¹ R. Reichelt, S. Günther, M. Röbber, J. Wintterlin, B. Kubias, B. Jakobi, and R. Schlögl, *Phys. Chem. Chem. Phys.* **9**, 3590 (2007).
- ²² H. A. Engelhardt and D. Menzel, *Surf. Sci.* **57**, 591 (1976).
- ²³ H. Albers, J. M. M. Droog, and G. A. Bootsma, *Surf. Sci.* **64**, 1 (1977).
- ²⁴ C. Benndorf, M. Franck, and F. Thieme, *Surf. Sci.* **128**, 417 (1983).
- ²⁵ R. B. Grant and R. M. Lambert, *Surf. Sci.* **146**, 256 (1984).
- ²⁶ D. Schmeisser and K. Jacobi, *Surf. Sci.* **156**, 911 (1985).
- ²⁷ C. T. Campbell, *Surf. Sci.* **173**, L641 (1986).
- ²⁸ M. E. M. Spruit, E. W. Kuipers, F. H. Geuzebroek, and A. W. Kleyn, *Surf. Sci.* **215**, 421 (1989).
- ²⁹ M. E. M. Spruit and A. W. Kleyn, *Chem. Phys. Lett.* **159**, 342 (1989).
- ³⁰ X.-D. Wang, W. T. Tysoe, R. G. Greenler, and K. Truszkowska, *Surf. Sci.* **257**, 335 (1991).
- ³¹ P. H. F. Reijnen, A. Raukema, U. van Slooten, and A. W. Kleyn, *Surf. Sci.* **253**, 24 (1991).
- ³² X. Bao, J. V. Barth, G. Lehmppfuhl, R. Schuster, Y. Uchida, R. Schlögl, and G. Ertl, *Surf. Sci.* **284**, 14 (1993).
- ³³ B. Pettinger, X. Bao, I. C. Wilcock, M. Muhler, and G. Ertl, *Phys. Rev. Lett.* **72**, 1561 (1994).
- ³⁴ F. B. de Mongeot, U. Valbusa, and M. Rocco, *Surf. Sci.* **339**, 291 (1995).
- ³⁵ A. Raukema, D. A. Butler, F. M. A. Box, and A. W. Kleyn, *Surf. Sci.* **347**, 151 (1996).
- ³⁶ X. Bao, M. Muhler, T. Schedel-Niedrig, and R. Schlögl, *Phys. Rev. B* **54**, 2249 (1996).
- ³⁷ S. Lacombe, F. Cemič, P. He, H. Dietrich, P. Geng, M. Rocca, and K. Jacobi, *Surf. Sci.* **368**, 38 (1996).
- ³⁸ M. Rocca, F. Cemič, F. Buatier de Mongeot, U. Valbusa, S. Lacombe, and K. Jacobi, *Surf. Sci.* **373**, 125 (1997).
- ³⁹ T. Schedel-Niedrig, X. Bao, M. Muhler, and R. Schlögl, *Ber. Bunsenges. Phys. Chem.* **101**, 994 (1997).
- ⁴⁰ W.-X. Li, C. Stampfl, and M. Scheffler, *Phys. Rev. B* **65**, 075407 (2002).
- ⁴¹ C. Stegelmann and P. Stoltze, *Surf. Sci.* **552**, 260 (2004).
- ⁴² A. Reicho, A. Stierle, I. Costina, and H. Dosch, *Surf. Sci.* **601**, L19 (2007).
- ⁴³ R. Reichelt, S. Günther, J. Wintterlin, W. Moritz, L. Aballe, and T. O. Menten, *J. Chem. Phys.* **127**, 134706 (2007).
- ⁴⁴ C. T. Campbell, *J. Phys. Chem.* **89**, 5789 (1985).
- ⁴⁵ C. T. Campbell, *J. Catal.* **94**, 436 (1985).
- ⁴⁶ S. A. Tan, R. B. Grant, and R. M. Lambert, *J. Catal.* **104**, 156 (1987).
- ⁴⁷ R. A. van Santen and H. P. C. E. Kuipers, *Adv. Catal.* **35**, 265 (1987).
- ⁴⁸ S. Hawker, C. Mukoid, J. P. S. Badyal, and R. M. Lambert, *Surf. Sci.* **219**, L615 (1989).
- ⁴⁹ C. Mukoid, S. Hawker, J. P. S. Badyal, and R. M. Lambert, *Catal. Lett.* **4**, 57 (1990).
- ⁵⁰ K. Wu, X. Wei, Y. Cao, D. Wang, and X. Guo, *Catal. Lett.* **26**, 109 (1994).
- ⁵¹ A. F. Carley, P. R. Davies, and M. W. Roberts, *Curr. Op. Sol. State Mat. Sci.* **2**, 525 (1998).
- ⁵² A. I. Boronin, V. I. Andeev, S. V. Koshcheev, K. T. Murzakhmetov, S. F. Ruzankin, and G. M. Zhidomirov, *Kinetics Catal.* **40**, 653 (1999).
- ⁵³ V. I. Avdeev and G. M. Zhidomirov, *Surf. Sci.* **492**, 137 (2001).
- ⁵⁴ K. C. Scheer, A. Ki, J. Kiss, and J. White, *Topics Catal.* **20**, 43 (2001).
- ⁵⁵ D. Stacchiola, G. Wu, M. Kaltchev, and W. Tysoe, *J. Mol. Catal. A: Chem.* **167**, 13 (2001).
- ⁵⁶ A. Klust and R. J. Madix, *Surf. Sci.* **600**, 5025 (2006).
- ⁵⁷ W. Gao, M. Zhao, and Q. Jiang, *J. Phys. Chem. C* **111**, 4042 (2007).
- ⁵⁸ J. R. B. Gomes, S. Gonzalez, D. Torres, and F. Illas, *Russ. J. Phys. Chem. B* **1**, 292 (2007).
- ⁵⁹ J. Greeley and M. Mavrikakis, *J. Phys. Chem. C* **111**, 7992 (2007).
- ⁶⁰ L. Zhou and R. J. Madix, *J. Phys. Chem. C* **112**, 4725 (2008).
- ⁶¹ W. Huang, Z. Jiang, and J. M. White, *Catal. Today* **131**, 360 (2008).
- ⁶² P. Christopher and S. Linic, *J. Am. Chem. Soc.* **130**, 11264 (2008).
- ⁶³ A. Klust and R. J. Madix, *J. Chem. Phys.* **126**, 084707 (2007).
- ⁶⁴ C. Stampfl, M. Ganduglia-Pirovano, K. Reuter, and M. Scheffler, *Surf. Sci.* **500**, 368 (2002).
- ⁶⁵ B. L. M. Hendriksen, S. C. Bobaru, and J. W. M. Frenken, *Surf. Sci.* **552**, 229 (2004).
- ⁶⁶ M. D. Ackermann, T. M. Pedersen, B. L. M. Hendriksen, O. Robach, S. C. Bobaru, I. Popa, C. Quiros, H. Kim, B. Hammer, S. Ferrer, et al., *Phys. Rev. Lett.* **95**, 255505 (2005).
- ⁶⁷ K. Reuter and M. Scheffler, *Phys. Rev. B* **73**, 045433 (2006).
- ⁶⁸ E. Lægsgaard, F. Besenbacher, K. Mortensen, and I. Stensgaard (1988).
- ⁶⁹ E. Uggerhøj, *Nucl. Instrum. Meth. Phys. Res. B* **99**, 261 (1995).
- ⁷⁰ K. C. Scheer, A. Kis, J. Kiss, and J. White, *Topics Catal.* **20**, 43 (2002).
- ⁷¹ W. X. Huang and J. M. White, *Catal. Lett.* **84**, 143 (2002).
- ⁷² W. X. Huang and J. M. White, *Langmuir* **18**, 9622 (2002).

- ⁷³ M.-L. Bocquet, P. Sautet, J. Cerda, C. I. Carlisle, M. J. Webb, and D. A. King, *J. Am. Chem. Soc.* **125**, 3119 (2003).
- ⁷⁴ W. X. Huang and J. M. White, *Surf. Sci.* **529**, 455 (2003).
- ⁷⁵ M. J. Webb, S. M. Driver, and D. A. King, *J. Phys. Chem. B* **108**, 1955 (2004).
- ⁷⁶ A. R. Alemozafar and R. J. Madix, *Surf. Sci.* **587**, 193 (2005).
- ⁷⁷ J. P. Perdew, K. Burke, and M. Ernzerhof, *Phys. Rev. Lett.* **77**, 3865 (1996).
- ⁷⁸ M. D. Segall, P. L. D. Lindan, M. J. Probert, C. Pickard, P. Hasnip, S. J. Clark, and M. C. Payne, *J. Phys.: Cond. Matt.* **14**, 2717 (2002).
- ⁷⁹ J. Tersoff and D. R. Hamann, *Phys. Rev. B* **31**, 805 (1985).
- ⁸⁰ F. Besenbacher, *Rep. Prog. Phys.* **59**, 1737 (1996).
- ⁸¹ H. Schubert, U. Tegtmeier, D. Herein, X. Bao, M. Muhler, and R. Schlögl, *Catal. Lett.* **33**, 305 (1995).
- ⁸² J. P. Biberian and M. A. van Hove, *Surf. Sci.* **138**, 361 (1984).
- ⁸³ In a previous communication¹⁹ we based the matrix notation on a different set of substrate unit vectors with an inscribed angle of 60° between the two unit vectors. Here we instead assume 120°. In the previously used notation the matrix is written $\begin{pmatrix} 3 & 0 \\ -4 & 5 \end{pmatrix}$.
- ⁸⁴ L. R. Merte, J. Knudsen, L. C. Grabow, R. T. Vang, E. Lægsgaard, M. Mavrikakis, and F. Besenbacher, *Surf. Sci.* **603**, L15 (2009).
- ⁸⁵ E. Lundgren, G. Kresse, C. Klein, M. Borg, J. N. Andersen, M. De Santis, Y. Gauthier, C. Konvicka, M. Schmid, and P. Varga, *Phys. Rev. Lett.* **88**, 246103 (2002).
- ⁸⁶ S. Helveg, W. X. Li, N. C. Bartelt, S. Horch, E. Lægsgaard, B. Hammer, and F. Besenbacher, *Phys. Rev. Lett.* **98**, 115501 (2007).